ACSNANO

www.acsnano.org

ARTICLE

Infant Skin Friendly Adhesive Hydrogel Patch Activated at Body Temperature for Bioelectronics Securing and Diabetic Wound Healing

Yanan Jiang,[#] Xin Zhang,[#] Wei Zhang,[#] Menghao Wang, Liwei Yan, Kefeng Wang, Lu Han,[*] and Xiong Lu[*]

Cite This: *ACS Nano* 2022, 16, 8662−8676

Read Online

ACCESS | Metrics & More | Article Recommendations | Supporting Information

ABSTRACT: **Adhesive-caused injury is a great threat for infants with premature skin or diabetic patients with fragile skin because extra-strong adhesion might incur pain, inflammation, and exacerbate trauma upon removal. Herein, we present a skin-friendly adhesive hydrogel patch based on protein−polyphenol complexation strategy, which leads to a thermoresponsive network sensitive to body temperature. The adhesion of the hydrogel is smartly activated after contacting with warm skin, whereas the painless detachment is easily realized by placing an ice bag on the surface of the hydrogel. The hydrogel exhibits an immunomodulatory performance that prevents irritation and allergic reactions during long-period contact with the skin. Thus, the hydrogel patch works as a conformable and nonirritating interface to guarantee nondestructively securing bioelectronics on infant skin for healthcare. Furthermore, the hydrogel patch provides gentle adhesion to wounded skin and provides a favorable environment to speed up the healing process for managing diabetic wounds.**

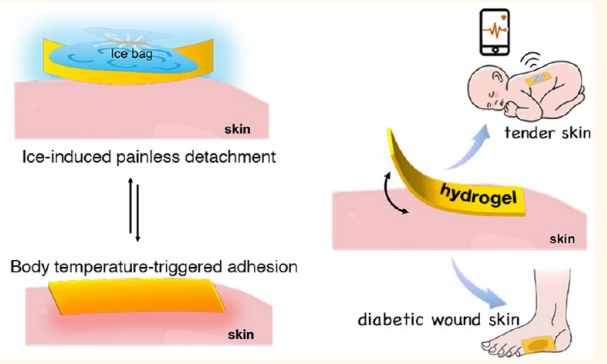

KEYWORDS: *diabetic wound, adhesive hydrogel, detachable hydrogel, polyphenol chemistry, wound dressing*

Skin adhesives are designed to offer intimate body contact applications, such as wound care, scar management, bioelectronics fixation, and transdermal patches for health monitoring or disease therapy.[1−4] However, most existing skin adhesives with strong adhesiveness are deemed aggressive and not suitable for application on fragile and sensitive skin, such as the skin of infants and diabetic patients.[5] Aggressive adhesive materials generally exacerbate pain and cause trauma during removal,[6] therefore delaying wound healing process, especially in the cases where daily reapplication is needed. For instance, patients with chronic wounds often suffer from painful wound dressing changes, and infants with delicate skin encounter frequent changes of caring patches or securing bioelectronics device. An alternative is to engineer skin adhesives with mild adhesiveness and trigger-detachable characteristics. Hydrogels with high water content and structural similarity to those of native skin tissue emerged as good candidates for fabricating soothing and gentle skin adhesives.[7] Triggerable detachment of the adhesive hydrogels can be achieved by applying chemical agents,[8−10] light irradiation,[11,12] electrical stimulus,[13] or heating[14] to cleave noncovalent or covalent adhesion bonds. However, these methods are harsh and not applicable for those sensitive, fragile, vulnerable, wounded, or ulcerated skins. Thus, it is important to design an ideal skin adhesive that exhibits adequate adhesion to remain intact for a desired duration time and offers painless detachment to avoid pain and trauma of the skin.

Contact-related skin irritation and allergies are other considerations related to adhesive material contacting the skin for a prolonged period.[6,15,16] Synthetic polymeric adhesives showed enough biocompatibility;[17] however, they pose the risk of leaching out residue onto the skin and causing irritation during long-term usage, which may render skin tissue prone to

Received: January 20, 2022
Accepted: May 9, 2022
Published: May 13, 2022

https://doi.org/10.1021/acsnano.2c00662
ACS Nano 2022, 16, 8662−8676

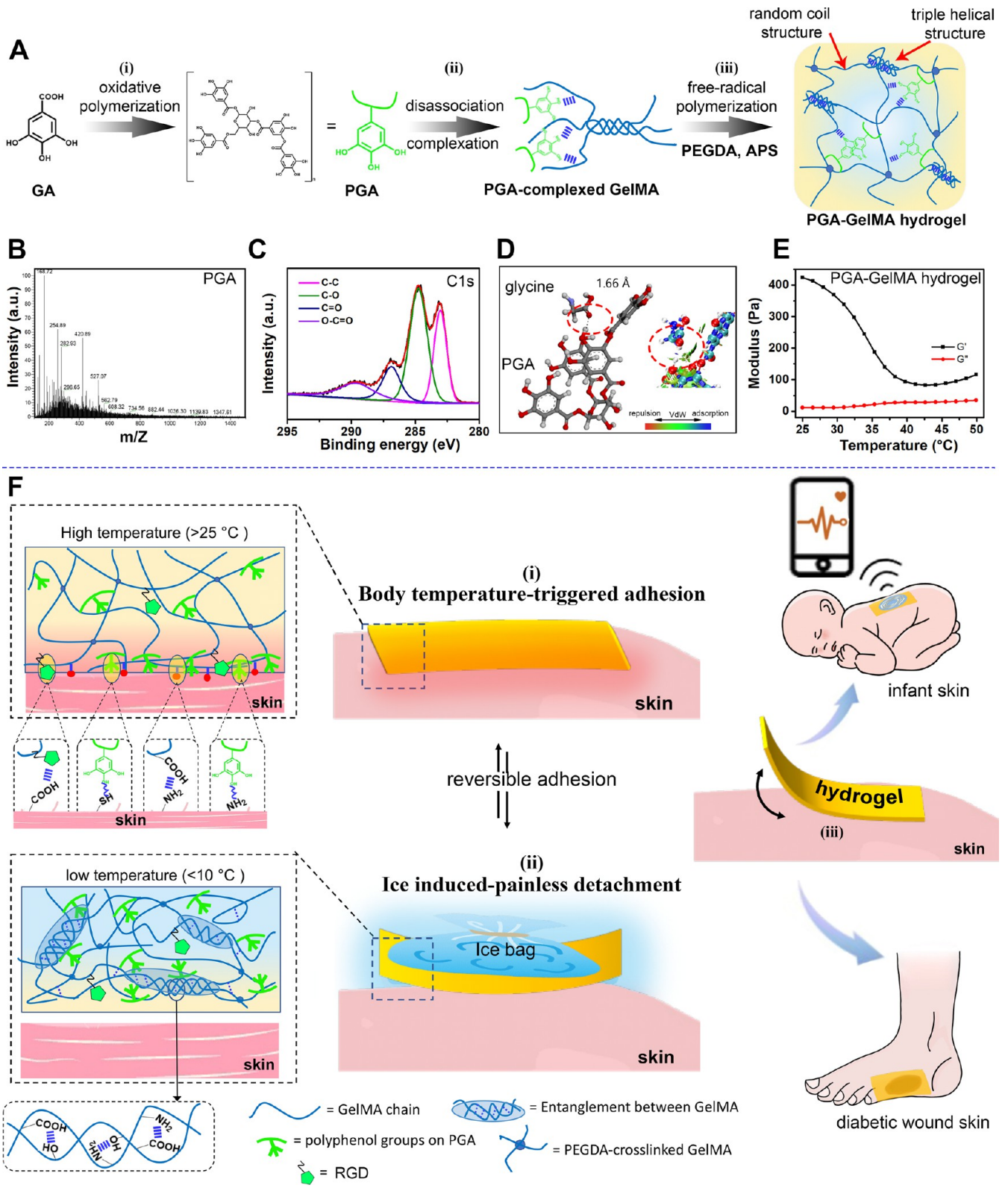

Figure 1. Design and characterization of a skin-friendly bioadhesive hydrogel providing nontraumatic adhesion and detachment. (A) Schematic diagram of the formation process of PGA-GelMA hydrogel. (i) Oxidative polymerization of GA to form PGA, (ii) PGA-complexed with GelMA chains, and (iii) hydrogel formation by GelMA chain polymerization. (B) Electrospray ionization/mass spectrometry (ESI/MS) analysis of PGA. (C) High resolution C 1s XPS spectra of PGA. (D) Density functional theory calculations demonstrating the interactions between PGA and glycine from GelMA chains. The color bar indicated the type and strength of the interactions. Blue meant notable adsorption and red meant notable repulsion, and green indicated the existence of van der Waals (VDW) interactions. (E) Temperature sweep showed storage modulus (G') and loss modulus (G'') of 1.3 wt % PGA-GelMA hydrogel between 25 and 50 °C under a constant strain amplitude of 1% and frequency of 1 Hz. (F) Schematic illustrations of the body temperature-triggered gentle adhesion and ice-cooling-induced painless detachment of the PGA-GelMA hydrogel.

https://doi.org/10.1021/acsnano.2c00662
ACS Nano 2022, 16, 8662−8676

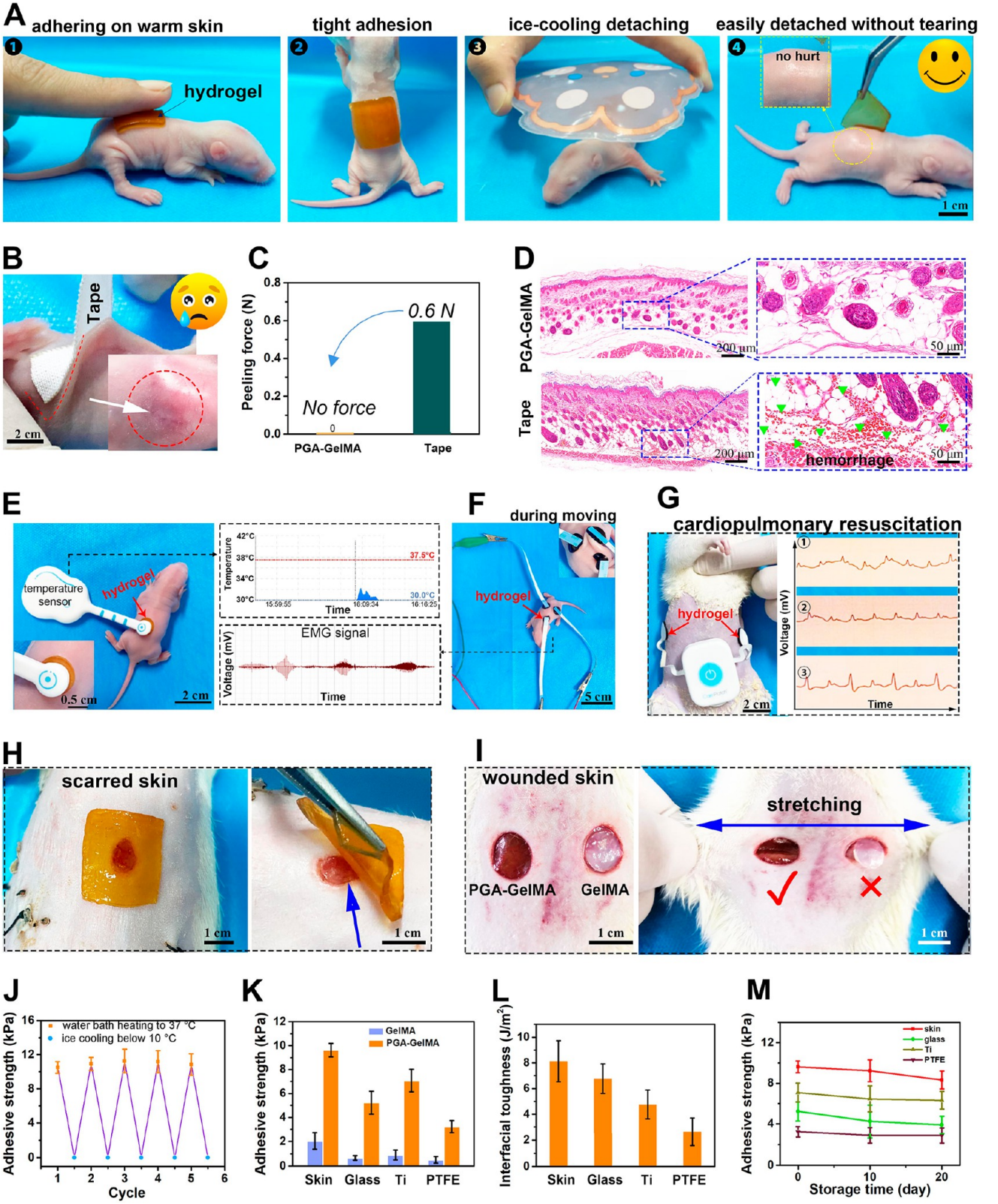

Figure 2. Body temperature-triggered adhesion and ice-cooling-induced detachment of the PGA-GelMA hydrogel. (A) Photographs of adhering and triggerable removal of the PGA-GelMA hydrogel on an infant rat skin surface. (B) A commercial medical tape caused pulling and severe damage on the skin during peeling. (C) Measured peeling forces for PGA-GelMA hydrogel and medical tape from infant rat skin. (D) H&E staining images of underlying skin tissues following removal of the PGA-GelMA hydrogel with the aid of ice cooling and the aggressive medical tape. Application of the conductive PGA-GelMA hydrogel as skin-friendly adhesive interfaces to mount various bioelectronics on the skin to detect biosignals, including (E) a wireless thermometer was amounted, inset showing the temperature tracking profile, (F) three bioelectrodes were fixed to record electromyographic (EMG) signal, (G) a wireless electrocardiogram (ECG) recorder was mounted for real-time heart signal detection during cardiopulmonary resuscitation (CPR) of a rat. (H) The hydrogel was adhered on a scarred skin for

https://doi.org/10.1021/acsnano.2c00662
ACS Nano 2022, 16, 8662−8676

Figure 2. continued

protection, which did not destroy scar during peeling (blue arrow). The hydrogel used in (F, G) contained 0.1 wt % PEDOT nanoparticles for improving conductivity. (I) The PGA-GelMA hydrogel tightly adhered to the surrounding tissue of full-thickness wound (diameter: 10 mm) to withstand stretching of the nearby skin, whereas the GelMA hydrogel without adhesiveness easily slip out. (J) Adhesive strengths of the PGA-GelMA hydrogel upon heating the hydrogel to 37 °C or cooling to 10 °C. (K) Comparison of adhesive strengths between PGA-GelMA and pure GelMA hydrogels. (L) Interfacial toughness of PGA-GelMA hydrogel to diverse substrates. (M) Long-term stable adhesiveness of the PGA-GelMA to diverse substrates. The GA content of PGA-GelMA hydrogels was 1.3 wt %.

trauma. Approaches such as encapsulation of antiallergic or anti-inflammatory drugs have been applied to address these concerns; however, they are often limited by complicated fabrication processes, high cost, drug side effects, and uncontrolled loading and release of the bioactive agents. Furthermore, drug-encapsulated adhesives are not suitable for babies, young children, and patients with chronic diseases who are very sensitive to medicine. Natural phenolic and polyphenol compounds (e.g., gallic acid, caffeic acid, tannic acid, and catechin) extracted from plants possess multiple biological functions, such as antioxidative, anti-inflammatory, and antiallergy activities,[18−21] and recent studies have shown that phenolic compounds can be used to construct strong adhesive materials through the coupling of quinone-nucleophile groups at the interface of the adhesive and various substrates.[22]

Herein, we reported a skin-friendly bioadhesive hydrogel patch that provided nonirritating adhesion and nontraumatic detachment, which was suitable for caring infants and patients who are very sensitive to medicine (Figure 1). The hydrogel was formed by a polyphenol−protein complexation strategy, and therefore the painless adhesion and detachment of the hydrogel could be simply triggered by body temperature and ice cooling, respectively. Meanwhile, the hydrogel exhibited excellent antioxidative and anti-inflammatory ability, which could intrinsically prevent skin irritation and allergic reactions. The hydrogel established a soft yet nonallergic interface with skin, which allowed nondestructive detachment and reattachment of epidermal bioelectronics on infant skin for reliable and long-term health caring. Furthermore, the hydrogel acted as an immunomodulatory wound dressing to accelerate diabetic wound healing in a nonpharmacological manner.

RESULTS AND DISCUSSION

Design Strategy. The skin-friendly adhesive hydrogel was prepared by complexation of polymerized gallic acid (PGA) with gelatin methacryloyl (GelMA), as shown in Figure 1A. First, gallic acids (GA) were oxidatively polymerized into PGA by atmospheric oxygen in the alkaline condition (Figure 1A-i). The phenolic groups on GA molecules were highly sensitive to oxidation and formed reactive pyrogallol-quinone groups, which further reacted with other GA molecules and polymerized into PGA oligomers. Second, PGA dissociated GelMA chains and complexed with the GelMA chains (Figure 1A-ii). Finally, the PGA-GelMA hydrogel was formed via free-radical polymerization of the GelMA chains (Figure 1A-iii) that were cross-linked by covalent and noncovalent interactions. The oxidative polymerization step to form PGA was critical for the formation of the hydrogel, because the large PGA molecule can interact with GelMA chains, whereas GA monomers retarded free-radical polymerization of GelMA chains to form a solid gel (Figure S1). PGA enriched with a large amount of phenolic and quinone groups, which synergistically enhanced the adhesion and cohesion of the GelMA network, endowing the hydrogel with adequate tissue adhesiveness. The electrospray ionization/mass spectrometry (ESI/MS) analysis showed strong signals at m/z 254.8 and 420.8, indicating the dimeric and trimeric structures in the polymerized GA, respectively (Figure 1B and Figure S2). The UV−vis spectra presented new broad absorption bands (260−290 and 335−370 nm) for PGA compared with those for GA (Figure S3b,c), also indicating the polymerization of GA to PGA under alkaline condition.[23,24] From the C 1s XPS spectra, the PGA obtained after 20 min of oxidization had a balanced number of phenolic and quinone groups (Figure 1C, Figure S3d−f, and Table S4), and this PGA was used to prepare the PGA-GelMA hydrogels.

The PGA-GelMA complexation tuned the cross-linking of GelMA network by introducing a high density of noncovalent bonds (Figure 1A-iii) and enabled the GelMA network response to thermal stimuli, resulting in temperature-triggered adhesion and detachment of the hydrogel. The interactions between PGA and GelMA chains was demonstrated by density functional calculations (Figure 1D, Figure S4, and Table S5), which identified that the interactions mainly occurred between the carbonyl/hydroxyl groups on GelMA chains and the polyphenol groups of PGA.[25] The complexation of PGA with GelMA chain entanglements prevented the renaturation of triple helical structure, and stabilized the gelatin chains in the randomly coiled state,[26,27] which could response to temperature changes. Dynamic temperature sweep measurements showed that both the storage (G') and loss (G'') moduli of the PGA-GelMA hydrogel decreased when the hydrogel temperature was raised above 30 °C (Figure 1E), confirming the thermal responsiveness of the PGA-GelMA hydrogel. Note that the change in storage modulus of the PGA-GelMA hydrogel was 72.6%, much higher than that of GelMA hydrogel (21.5%) (Figure S5). This result supported that the PGA complexion tuned the cross-linking of GelMA network and increased the degree of freedom for the gelatin chains to form the PGA-GelMA hydrogel with coordinated physical and chemical cross-linking, which was different from the case for the pure GelMA hydrogel that was chemically cross-linked by irreversible bonds.[28] In addition, the storage modulus of the PGA-GelMA hydrogel was higher than loss modulus during the temperature sweep, indicating the solid-like elasticity of the hydrogel, which could remain in the solid state instead of a viscous liquid at 35 °C (Figure S6). Once the PGA-GelMA hydrogel was in contact with warm skin surfaces, the body temperature triggered the decomplexation of GelMA chains, and the mobility of the GelMA chains in the hydrogel was promoted to make a soft hydrogel, which could readily conform to the target tissue surface. Then the freely movable GelMA in the hydrogel chains would expose abundant reactive motifs, such as amino groups and carboxyl groups, which synergistically worked with phenolic groups to form multiple interfacial bonding on the skin surface, resulting in strong adhesion (Figure 1F-i). Upon cooling by an ice bag, the GelMA chains re-entangled because of the formation of intermolecular hydrogen bonds, and therefore the freedom of movement of the gelatin chains was drastically reduced, which cleaved the

https://doi.org/10.1021/acsnano.2c00662
ACS Nano 2022, 16, 8662−8676

adhesion bonding at the molecular level. Meanwhile, the intermolecular hydrogen bonds between re-entangled GelMA chains increased the cross-linking density in the PGA-GelMA network, leading to a rigid hydrogel, which was difficult to conformably contact the tissue surface to form interfacial interactions at the interface. Thus, the hydrogel was nondestructively detached from the skin surface without leaving any residue upon cooling (Figure 1F-ii). Thus, the PGA-GelMA hydrogel offers an extra-gentle, less-painful, and nonallergic way to mount bioelectronics on the infant skin for contacting healthcare, as well as an adhesive patch to promote diabetic wound management (Figure 1F-iii).

Temperature-Triggered Painless Adhesion and Detachment. To evaluate the temperature-responsive adhesion of the hydrogel to the skin tissue, the PGA-GelMA hydrogel was applied on the dorsal skin of a naked infant rat, followed by ice-cooling-triggered detachment of the hydrogel (Figure 2A). The hydrogel adhered to the warm skin of the rat after being pressed for 10 s, forming a conformable and seamless contact with the corrugated skin surface. The adhesion was strong enough to accommodate skin deformation during rat movements (Figure 2A-1,2). To detach the hydrogel from the skin, an ice bag was applied to cool the hydrogel for 10 s, and then the hydrogel was self-detached without hurting the skin and leaving residues (Figure 2A-3,4). For comparison, a commercial medical adhesive tape was used, which showed strong binding to the skin, and its detachment required a large peeling force that made the skin red and swollen (Figure 2B,C). After the removal of the tape, the underlying skin tissue was further analyzed by hematoxylin and eosin (H&E) staining, and the results showed heavy subcutaneous hemorrhage and delamination in the dermis. In contrast, the skin tissue under the PGA-GelMA hydrogel remained intact, similar to the sham skin region (Figure 2D). In addition, the hydrogel was nonallergenic and nonirritating to the infant skin even after long-term (12 h) adhesion, as demonstrated by gross observation (Figure S7A). Histological analysis further revealed that no lesions, such as erythema, infiltration, and immune response, occurred in the stratum corneum, epidermis, and dermis (Figure S7B). These results confirmed that the hydrogel was skin-friendly and achieved nonallergenic adhesion and nondestructive detachment.

Because of its temperature-triggered adhesion and detachment, the PGA-GelMA hydrogel can be conveniently applied as a biointerfacing material to enable seamless mounting of epidermal bioelectronics on delicate skin surfaces. To demonstrate this point, an adhesive and conductive hydrogel was fabricated by incorporation of PEDOT NPs into the PGA-GelMA hydrogel (Figure S8), which exhibited a high conductivity of 15.4 S/m and an adhesive strength of 8.5 kPa. The adhesive and conductive hydrogel enabled gentle and conformal attachment of a wireless thermometer and bioelectrodes on the dorsal skin of an infant rat for remote and long-term tracking of its body temperature and electromyographic (EMG) signal (Figure 2E,F). The bioelectrodes were firmly fixed on the skin of the rat when the rat was climbing. In another example, a commercial electrocardiogram (ECG) recorder was fixed on the chest skin of a rat by using a thin hydrogel as an adhesive layer to record ECG signals during cardiopulmonary resuscitation (CPR) of the rat (Figure 2G and Movie S1). In both cases, the sensors remained stable on the skin to remotely record signals over a long period of time without lesions and were easily removed from the skin after ice cooling without causing irritation. These results demonstrated that the PGA-GelMA hydrogel was a biocompatible and antiallergenic skin adhesive for integration with epidermal bioelectronics. Application of the PGA-GelMA hydrogel could potentially overcome the shortcomings of conventional aggressive adhesives used, which caused pulling and stretching of the hair and skin during removal (Figure S9). Such PGA-GelMA hydrogel integrated bioelectronics are especially suitable for babies, children, and elderly people whose skin is very vulnerable and sensitive to adhesive materials. The PGA-GelMA hydrogel with nondestructive adhesion also showed advantages for wound care. As shown in Figure 2H and Movie S2, the hydrogel stuck on the fragile scarred skin and was easily removed without pulling the skin and traumatizing the wound bed after ice-cooling for 10 s. Furthermore, the PGA-GelMA hydrogel adhered to the fresh wound to seal the wound site on the dorsum of rats (Figure 2I and Movie S3). Prior to implanting the hydrogel into the wound sites, the excessive biofluid around the injured wound was gently removed by a dry gauze. After the hydrogel was applied at the wound sites, the hydrogel could directly contact with the tissue surfaces and immediately form multiple interfacial bonds between abundant reactive motifs on the hydrogel (such as phenolic groups, quinone groups, amino groups, or carboxyl groups) and amine or thiol groups on the warm tissue surfaces. Thus, the PGA-GelMA hydrogel showed strong adhesion to the surrounding tissue of the wound site even after extensive distortion (stretching or twisting) of the adjacent skin, which was superior to the nonadhesive GelMA hydrogel that was easily split from the wound site upon small skin deformation.

The PGA-GelMA hydrogel displayed stable cyclic temperature-triggered adhesion and detachment, which satisfied the need for repeated application in daily life. As demonstrated by five cycles of repeated adhesion tests on the porcine skin under temperature variation, the hydrogel maintained a high average adhesive strength (10 kPa) at 37 °C, whereas it completely lost its adhesion at 10 °C (Figure 2J). The adhesive property of the PGA-GelMA hydrogel was also determined by the content and the oxidation time of PGA, and the adhesive strength of PGA-GelMA hydrogel significantly increased from 2.0 ± 1.6 to 10.8 ± 8.5 kPa as the PGA content was increased from 0 to 2 wt % (Figure S10a). The adhesive strength of PGA-GelMA hydrogel dramatically decreased to 1.16 ± 0.65 kPa when the oxidation time of PGA was increased 12 h (Figure S10b), which was because long-term oxidation caused the overconsuming of phenolic moieties.[29] The PGA-GelMA hydrogel also showed universal adhesion to a wide variety of substrates, including hydrophilic glass slides, hydrophobic PTFE, and metal (Ti) substrates (Figure 2K). The versatile adhesion behavior of the PGA-GelMA hydrogel was ascribed to the abundant phenolic groups in the hydrogel, which had high reactivity to interact with different types of substrates via hydrogen bonding, hydrophobic interactions, $\pi-\pi$ interactions, or metal coordination.[30−34] The adhesion energy of the PGA-GelMA hydrogel to porcine skin, glass, Ti, and PTFE substrates was found to be 8.1, 6.8, 4.8, and 2.6 J/m^2, respectively (Figure 2L and Figure S11), which showed a trend similar to that of the adhesive strength. The adhesion energy of the PGA-GelMA hydrogel to tissues was at the same level as that of previously reported nanoparticle-based adhesive,[35] mussel-inspired adhesive,[36] and commercial adhesives (fibrin glue[37] or PEG-based adhesives[38]). It should be noted that the hydrogel exhibited higher adhesion to skin tissue than to other substrates, because the good adhesiveness of the hydrogel was attributed to both the abundant phenolic groups

https://doi.org/10.1021/acsnano.2c00662
ACS Nano 2022, 16, 8662−8676

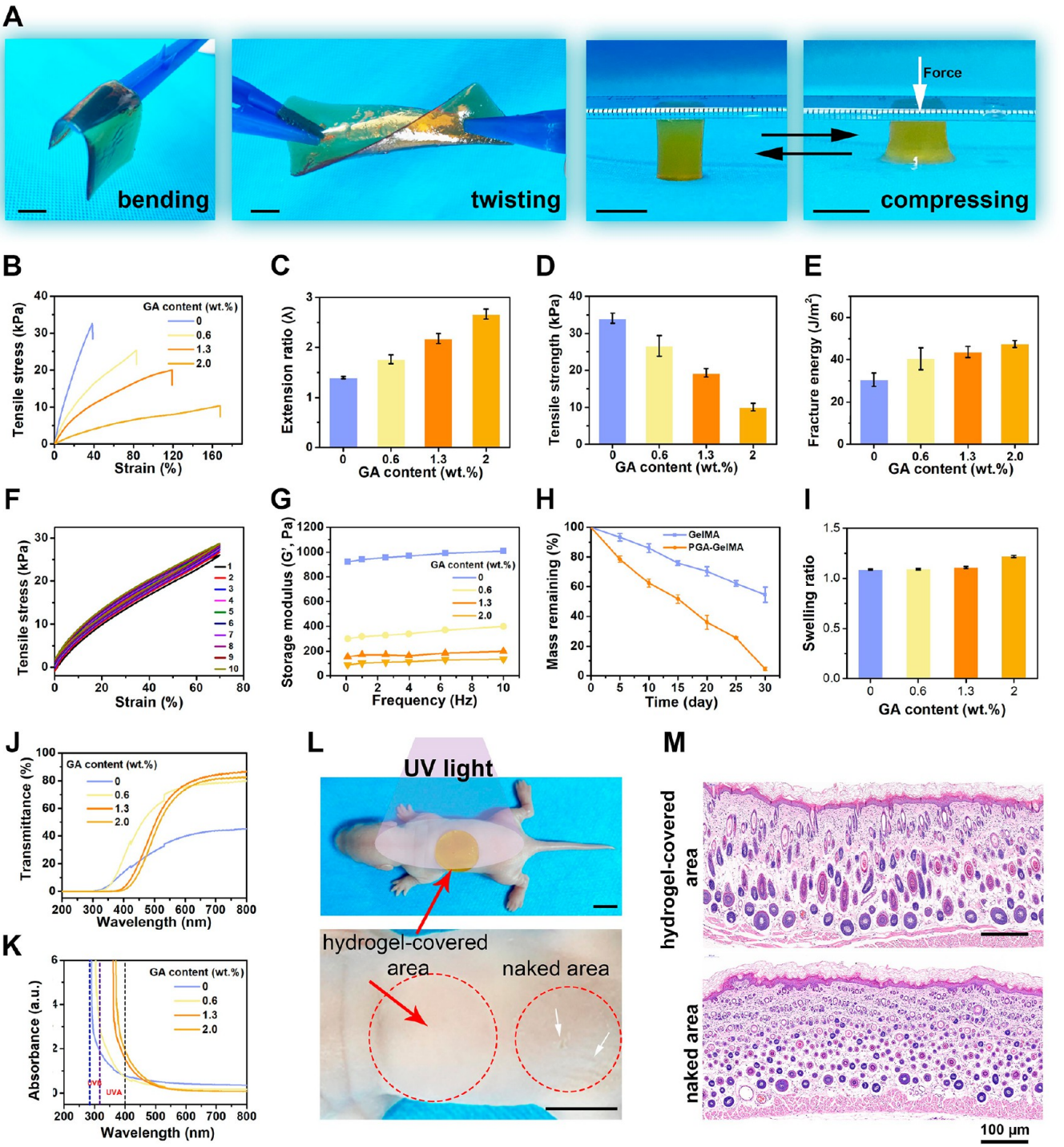

Figure 3. Physical properties of the PGA-GelMA hydrogel. (A) Photos showing the flexibility of hydrogel to bear bending, twisting, and compression. Scale bar: 1 cm. (B) Typical tensile stress−strain curves, (C) extension ratio, (D) tensile strength, and (E) fracture energy of PGA-GelMA hydrogels with various GA contents. (F) Successive loading−unloading tensile tests of the 1.3 wt % PGA-GelMA hydrogel for 10 cycles at a strain of 70%. (G) Dynamic storage modulus (G') of PGA-GelMA hydrogels as a function of frequency measured at a fixed strain of 1% (within the linear range). (H) Degradation behavior of the hydrogels (GelMA and 1.3 wt % PGA-GelMA) in the presence of 2 μg/mL collagenase. (I) Swelling ratio of the hydrogels in phosphate buffered solution (PBS, pH = 7.4). (J) UV−vis transmittance and (K) absorption spectra of PGA-GelMA hydrogels with various GA contents. (L) Photos of the 1.3 wt % PGA-GelMA hydrogel covering on the back skin of an infant rat for UV-shielding (top) and the skin after UV irradiation (bottom). White arrows show that the naked skin was dried and wrinkled. Scale bar: 1 cm. (M) H&E staining images of naked skin and the skin protected by the PGA-GelMA hydrogel.

and RGD motif in the hydrogel (Figure 1F), and RGD preferred to form multiple specific noncovalent interactions with tissue surfaces.[39,40] In addition, the hydrogel exhibited long-term stable adhesiveness to various substrates, even after 20 days of storage in a sealed container (Figure 2M). The adhesion durability of the PGA-GelMA hydrogel was further investigated by 10 cycles of adhesion-tensile tests. The results showed no loss in adhesive strength was observed during all 10 cyclic tests

https://doi.org/10.1021/acsnano.2c00662
ACS Nano 2022, 16, 8662−8676

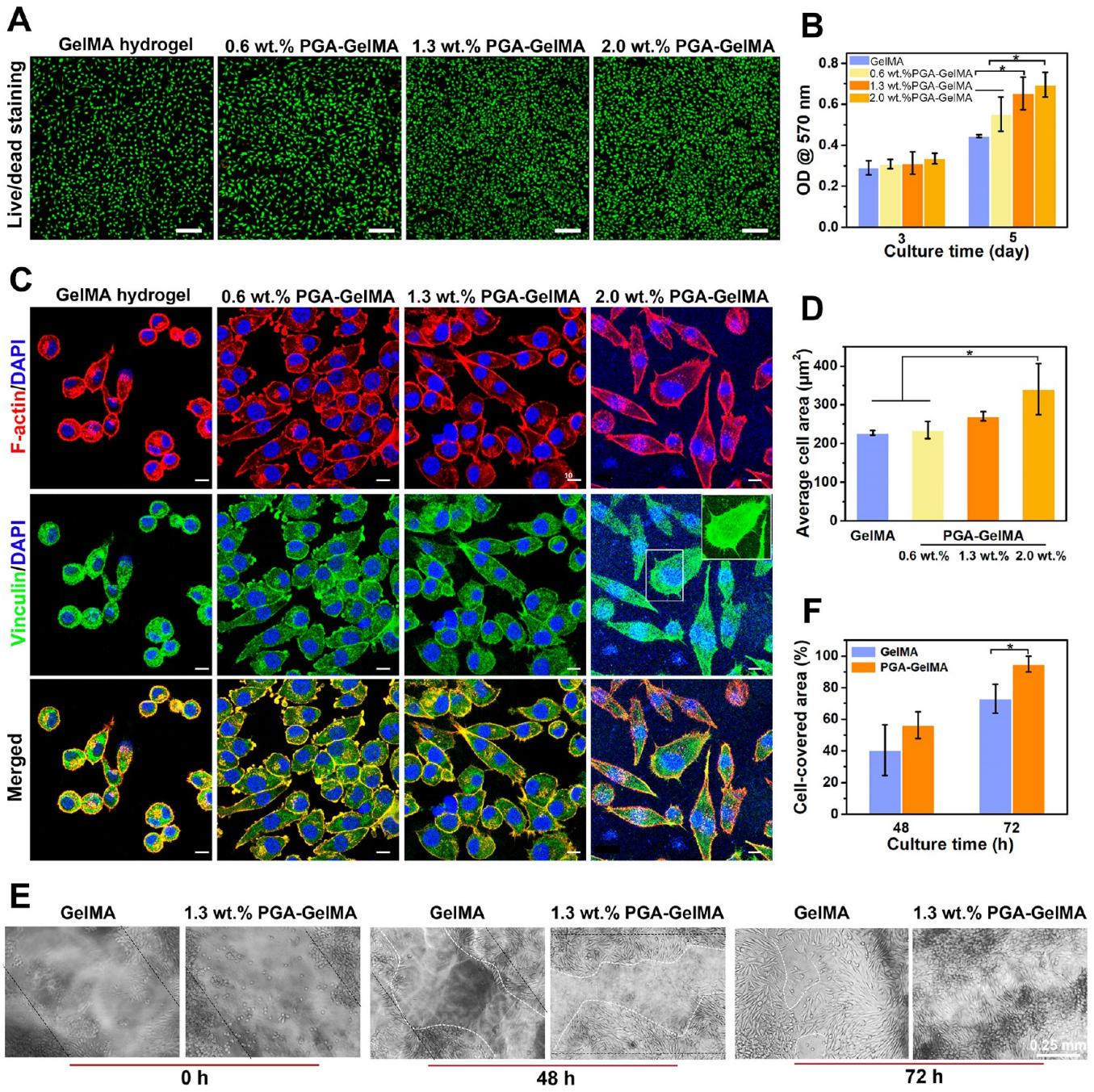

Figure 4. Evaluation of cell affinity of the PGA-GelMA hydrogel. (A) Live/dead staining for cell viability assay of L929 fibroblasts cultured on the various hydrogels. Live cells were stained in green, and dead cells were stained in red. Scale bar: 100 μm. (B) MTT assay of cell proliferation after 3 and 5 days of culturing on different hydrogels. (C) Confocal fluorescence microscopic images of focal adhesion protein and F-actin in L929 fibroblasts cultured on different hydrogels for 3 days. F-actin was stained with Phalloidin (red). Focal contacts were stained using Alexa Fluor 488 Rabbit monoclonal anti-Vinculin antibody. Cell nuclei were counterstained with DAPI. Scale bar: 100 μm. (D) Quantification of cell area of L929 fibroblasts on various hydrogels. (E) Representative phase-contrast images of L929 fibroblasts migration to the scratched area on GelMA and PGA-GelMA (1.3 wt %) hydrogels at time intervals of 0, 48, and 72 h. (F) Quantification of cell-covered area after 48 and 72 h of culturing. *$p < 0.05$.

(Figure S12), implying the excellent adhesion durability of the hydrogel for long-term and repeatable applications. Comparisons between the PGA-GelMA hydrogel and commercial adhesives in terms of the adhesive strength, on demand detachment, temperature-responsibility, and mechanical performances are provided in Table S6. The above findings validated that the PGA-GelMA hydrogel could be used as a gentle wound-care dressing with high adhesiveness and easy-to-detach ability, which could provide a solution for fragile skin wound caring and be suitable for wearable monitoring and medical device attachments.

Mechanical Flexibility and Recoverability. The PGA-GelMA hydrogel exhibited excellent flexibility and mechanical softness, which ensured its conformal contact on curved body surfaces and adaption to the dynamic movement of the skin to achieve seamless adhesion. As shown in Figure 3A, the PGA-

https://doi.org/10.1021/acsnano.2c00662
ACS Nano 2022, 16, 8662−8676

GelMA hydrogel was flexible and could be twisted and compressed, which was different from the case for the fragile pure GelMA hydrogels. Tensile tests indicated that the PGA-GelMA hydrogel had good stretchability (~160%) (Figure 3B), which was higher than that of human skin (60%−75%).[41,42] Complexation of PGA enhanced the elongation ratio of the hydrogels (Figure 3C) but decreased the tensile and compressive strengths (Figure 3D and Figure S13a). The fracture toughness of the PGA-GelMA hydrogel was evaluated using a single-edge notched test, and the results showed that the PGA-GelMA hydrogel displayed a fracture energy of 43 J m^{-2}, which was higher than that of the GelMA hydrogel (30 J m^{-2}) (Figure 3E). To further evaluate the recoverability and robustness of the hydrogels, 10 cycles of tensile loading−unloading tests with 10 s pausing between each cycle were carried out by applying a constant strain of 70%. A similar hysteresis curve was observed for all cycles (Figure 3F), demonstrating that the hydrogel had good fatigue resistance and constant energy dissipation during cyclic deformation. The cyclic compressive tests showed similar patterns (Figure S13b). Dynamic frequency measurements under the sweeping mode demonstrated that the storage modulus (G') of the hydrogels decreased following the addition of PGA (Figure 3G), indicating that the softness of the PGA-GelMA hydrogel increased with the increase of the PGA content. The prominent flexibility, softness, recoverability, and fatigue resistance of the PGA-GelMA hydrogel was ascribed to the multiple molecular interactions between PGA and GelMA chains (Figure 1A). The reactive polyphenol moieties on the PGA destroyed part of the intramolecular bonds between the GelMA chains and generated more intermolecular cross-links within the GelMA network, playing a tanning effect on the GelMA chains.[25,43,44] The excellent mechanical performances of PGA-GelMA hydrogel cannot be achieved by existing commercial products (Table S6), such as the fibrin-based Tissel exhibiting relatively low mechanical strength[45] and the PEG-based COSEAL adhesive being mechanically brittle.[4] Consequently, the PGA-GelMA hydrogel displayed superior mechanical properties, which made it mechanically compatible for use as bioadhesive patch on soft human skin.

Biodegradability and Swelling Behavior. The PGA-GelMA hydrogel was biodegradable, showing great competitiveness for commercial synthetic polymer-based skin adhesive products. The in vitro degradation of the PGA-GelMA and GelMA hydrogels was investigated by incubating them in collagenase type II solution (2 μg/mL) for up to 30 days (Figure 3H). The PGA-GelMA hydrogel showed a higher degradation rate than the GelMA hydrogel, which was because PGA complexation lowered the cross-linking density between the GelMA network and allowed larger swelling of the hydrogel and faster diffusion of collagenase to break the GelMA chains. As shown in Figure 3I and Figure S13c, the PGA-GelMA hydrogel had a swelling ratio slightly higher than that of the pure GelMA hydrogel, indicating the water absorption capacity of the PGA-GelMA hydrogel, whereas the small swelling ratio (<2) of the PGA-GelMA hydrogel (1.3 wt % PGA) could prevent the detachment of hydrogel from wet wound tissues during in vivo implantation.[46] The PGA-GelMA hydrogel lost 50% of the weight after 15 days of incubation and 100% of the weight after 30 days, demonstrating that the PGA-GelMA hydrogel could be completely degraded under physiological conditions. In short, the PGA-GelMA hydrogel with low swelling ratio and suitable biodegradation rate is advantageous for the implementation as an adhesive patch, which provides tissue integration at the initial stage and allows new tissue regeneration at a later stage.

Transparency and UV Shielding. Transparency is an important requirement for a skin adhesive patch to enable visual examination and allow patients under self- or home-care to easily check the underlying skin status.[47,48] The PGA-GelMA hydrogel displayed high transparency, as the UV−vis transmittance spectra exhibited an increasing trend in the wavelength range 400−800 nm (Figure 3J). In addition, the transmittance of the PGA-GelMA hydrogels declined sharply in the UV region below 400 nm (Figure 3K), and therefore the PGA-GelMA hydrogel had the ability to shield the UV light because of the UV absorption ability of polyphenolic motifs in the hydrogel.[49] The UV-shielding performance of the PGA-GelMA hydrogel was further demonstrated by attaching the hydrogel on the back skin of an infant rat for 2 min of UV irradiation. After UV irradiation, the skin covered by the PGA-GelMA hydrogel remained intact, whereas the skin directly exposed to UV light was heavily injured with dried and wrinkled surfaces (Figure 3L), and ruptured collagen fibers in the dermis (Figure 3M). In short, the PGA-GelMA hydrogel with high transparency and UV shielding ability can act as a skin adhesive to facilitate daily wound care and protect the skin from solar irradiation and photoaging.

Cell Adhesion on PGA-GelMA Hydrogel. The adhesive PGA-GelMA hydrogel was cytocompatibility and cell-affinitive and therefore can be used as a bioactive dressing to facilitate cell attachment and migration at injured sites. L929 fibroblasts were seeded on PGA-GelMA hydrogels and their viability and proliferation were evaluated using live/dead analysis and MTT assays. The fluorescent images revealed that the cells on all hydrogels exhibited high viability after 3 days of culture (Figure 4A), indicating good biocompatibility of the PGA-GelMA hydrogels. In addition, the number of live cells was higher on the PGA-GelMA hydrogels than those on the pure GelMA hydrogels. The MTT assay confirmed that the proliferation rate of cells on PGA-GelMA hydrogels was higher than that of GelMA hydrogel after 5 days of culture (Figure 4B). The good cytocompatibility of the hydrogel was attributed to phenolic group-mediated cell−matrix interaction.[50,51]

The cell actin cytoskeleton was further examined to characterize cell−matrix interactions by double staining cells with TRITC-phalloidin against F-actin and antibodies against vinculin after 3 days of culture. As shown in Figure 4C, L929 fibroblasts on GelMA hydrogels exhibited a round morphology and had relatively few vinculin-positive focal adhesions that only presented surrounding nuclei, suggesting minimal interactions with the GelMA matrix. In contrast, the cells on the PGA-GelMA hydrogels exhibited a spread morphology. The cells on the PGA-GelMA hydrogels with high GA contents (1.3 and 2 wt %) were noted, as they were fully elongated with many bright vinculin-positive focal adhesions at the outer edge of the actin structure. Merged images illustrated the colocalization of F-actin with focal adhesion proteins near the cell surface, suggesting that the cells could perceive and interact with the PGA-GelMA hydrogels. The quantified cell area confirmed that the PGA-GelMA hydrogel was able to increase cell adhesion (Figure 4D). Cell attachment to the hydrogels was further observed by a scanning electron microscope (SEM). SEM images showed that the cells on GelMA hydrogels displayed an aggregated morphology with a round shape, indicating that the cells minimized their contact with the hydrogel (Figure S14a,b). In contrast, the cells on PGA-GelMA hydrogels exhibited a flattened and spindle-like healthy morphology with extended

https://doi.org/10.1021/acsnano.2c00662
ACS Nano 2022, 16, 8662−8676

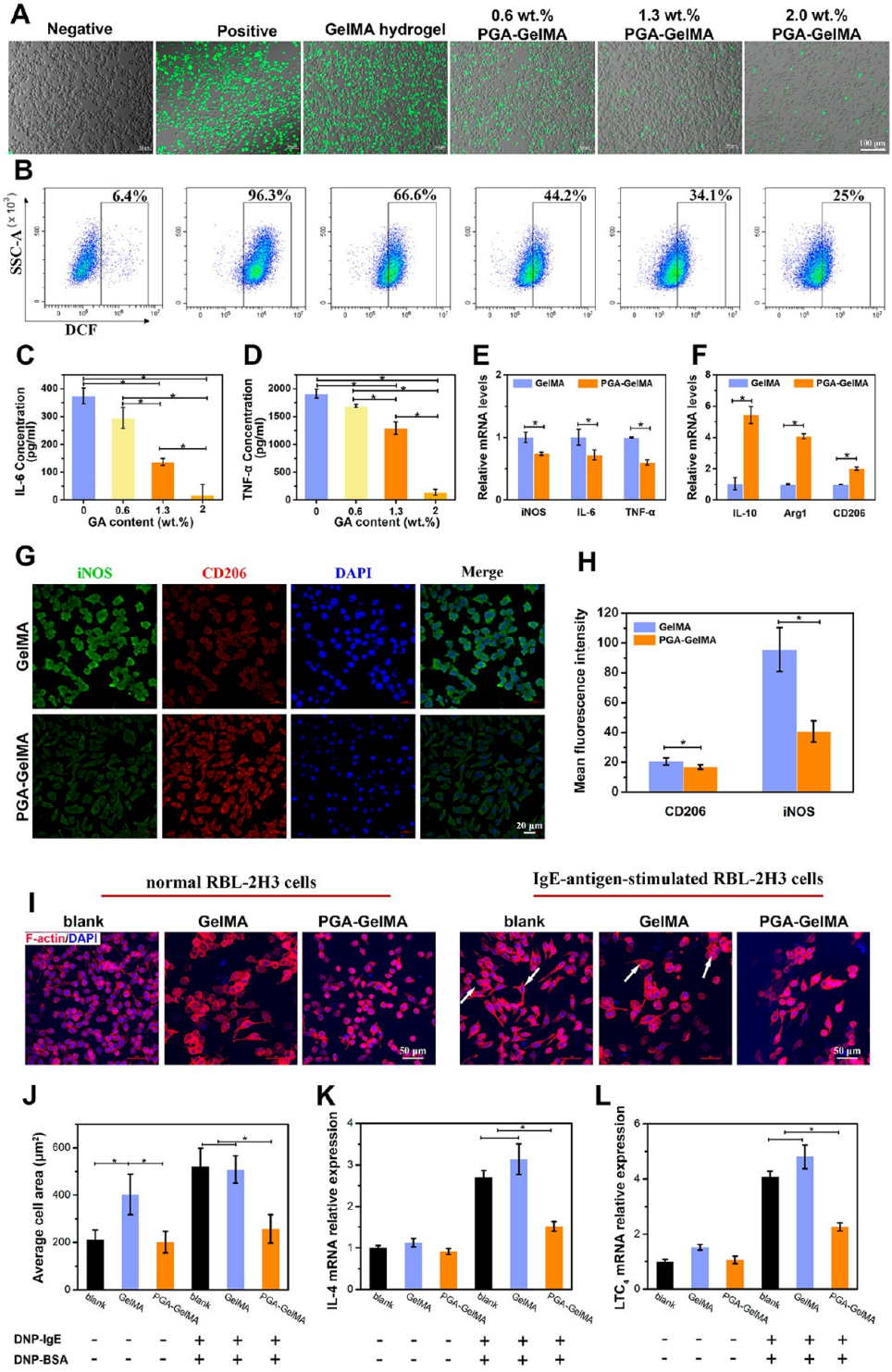

Figure 5. In vitro evaluation of antioxidative, anti-inflammatory, and antiallergic ability of PGA-GelMA hydrogel. (A) Representative ROS staining (green fluorescence) images of RAW264.7 macrophages under different treatment conditions. (B) Flow cytometry analysis of ROS levels in untreated and PGA-GelMA hydrogels-treated RAW264.7 macrophages incubated with 50 μM H_2O_2. Quantification of pro-inflammatory cytokines (C) IL-6 and (D) TNF-α of macrophages after treatment with PGA-GelMA hydrogels with various GA contents. The relative mRNA levels of (E) pro-inflammatory cytokines (iNOS, IL-6, TNF-α) and (F) anti-inflammatory markers (IL-10, Arg1, CD206) in macrophages treated with GelMA and 1.3 wt % PGA-GelMA hydrogels in the presence of lipopolysaccharide. (G) Macrophage polarization induced by a 1.3 wt % PGA-GelMA hydrogel analyzed by immunofluorescence staining of iNOS (green, M1 macrophages marker) and CD206 (red, M2 macrophages marker) in macrophages. Cell nuclei were stained with DAPI (blue). (H) Mean fluorescence intensity of iNOS and CD206 from the immunofluorescence images in (G). (I) F-actin staining of RBL-2H3 cells on different samples with or without IgE-antigen complex stimulation. Arrows indicate the irregular cell morphology because of disassembly of the F-actin cytoskeleton. (J) Quantification of cell area of RBL-2H3 cells on various samples (blank, GelMA and 1.3 wt % PGA-GelMA) under different conditions. The effects of the hydrogels on the mRNA relative expression levels of (K) IL-4 and (L) LTC_4 in RBL-2H3 cells by complex stimulated with or without IgE-antigen. *$p < 0.05$.

https://doi.org/10.1021/acsnano.2c00662
ACS Nano 2022, 16, 8662−8676

lamellipodia and filopodia (Figure S14c,d), confirming that the PGA-GelMA hydrogels favored cell adhesion and spreading.

The PGA-GelMA hydrogels also supported the migration of fibroblasts to the scratched area, as demonstrated by an in vitro scratch assay (Figure 4E). Quantitative analysis revealed that the migration of fibroblasts on the PGA-GelMA hydrogel was faster than that of the cells on the GelMA hydrogel. After 72 h of culturing, the cell-covered area of the PGA-GelMA hydrogel was significantly higher than that of the GelMA hydrogel (Figure 4F), suggesting that the PGA-GelMA hydrogel promoted the migration process of L929 fibroblasts and induced fast closure of the cell-free gap. The in vitro cell culture results revealed that the complexation of PGA with GelMA enhanced the cell affinity of the hydrogel, facilitating the extension of cell protrusions, such as lamellipodia and filopodia, and in turn promoted cell spreading, proliferation, and migration, which was beneficial for the wound healing process.

Antioxidative and Anti-inflammatory Ability. The PGA-GelMA hydrogel exhibited antioxidative properties to scavenge reactive oxygen species (ROS) and therefore protect cells from ROS-mediated oxidative damage. To confirm the antioxidative property of the PGA-GelMA hydrogel, a free radical scavenging experiment was performed using the classic 1-diphenyl-2-picrylhydrazyl (DPPH) radical assay. From the UV−vis spectra, it was observed that the absorbance at 517 nm decreased with the increase of PGA content in the hydrogels (Figure S15a). After 90 min of incubation, more than 60% of the free radicals were eliminated by the PGA-GelMA hydrogel (2.0 wt % GA), which was much higher than that of the GelMA hydrogels (Figure S15b). Raw 264.7 cells were further cultured to examine the intracellular ROS scavenging ability of the PGA-GelMA hydrogel. As shown in Figure 5A, the intracellular ROS level (green fluorescent signal) of cells cultured in the GelMA hydrogel groups increased dramatically after treatment with 50 μM H_2O_2. In contrast, the intracellular ROS level significantly decreased when the cells were cultured with the PGA-GelMA hydrogel, and less fluorescence was observed on the PGA-GelMA hydrogel with 2.0 wt % GA, indicating the dose-dependent intracellular ROS scavenging activities. Quantitative analysis of intracellular ROS levels by flow cytometry further confirmed this observation (Figure 5B). The above results demonstrated that adequate contents of PGA in the hydrogel were essential for relieving the oxidative stress of the cells, which was attributed to the presence of the reductive phenolic groups on PGA that acted as electron donors and interacted with radicals.[52,53]

Furthermore, the PGA-GelMA hydrogel possessed anti-inflammatory and immunomodulatory properties. To demonstrate this point, the effect of PGA-GelMA hydrogels on RAW 264.7 macrophages was investigated in the presence of lipopolysaccharide (LPS). ELISA results indicated that the PGA-GelMA hydrogel significantly reduced the release of inflammatory cytokines (IL-6 and TNF-α) of macrophages (Figure 5C,D). Immunofluorescent staining was used to identify M1 and M2 macrophages after 48 h of culture on different hydrogels. Inducible nitric oxide synthase (iNOS) and CD206 (a mannose receptor) were stained to indicate M1 and M2 macrophage phenotypes, respectively (Figure 5G). The number of iNOS-labeled M1 macrophages was lower, and that of CD206-labeled M2 macrophages was higher on the PGA-GelMA hydrogel than on the GelMA hydrogel (Figure 5H). The phenotype of macrophages on the hydrogels was further evaluated by measuring the expression levels of pro-inflammatory (iNOS, IL-6, and TNF-α) and anti-inflammatory markers (IL-10, Arg1, and CD206). As shown in Figure 5E, the expression levels of iNOS, IL-6, and TNF-α were significantly decreased in macrophages treated with the PGA-GelMA hydrogel, in contrast to the GelMA hydrogel. Meanwhile, the expression levels of IL-10, Arg1, and CD206 were elevated in macrophages treated with the PGA-GelMA hydrogels (Figure 5F). These findings confirmed that the PGA-GelMA hydrogels alleviated the inflammatory response and effectively drove macrophage polarization to an anti-inflammatory phenotype, which were essential features to avoid irritative and allergic reactions after adhering on skin.

Antiallergic Ability. The PGA-GelMA hydrogels also exhibited antiallergic ability that could prevent ovalbumin-induced allergic reaction. To investigate the antiallergic effect of the hydrogel, the in vitro cellular model of IgE-mediated mast cell degranulation was used, and the RBL-2H3 cell line was chosen for the model. After being seeded on the hydrogels, the RBL-2H3 cells were sensitized by antidinitrophenyl IgE (DNP-IgE) for 24 h and then challenged with DNP-conjugated bovine serum albumin (DNP-BSA) for 1 h to induce degranulation. Since the membrane ruffling of stimulated mast cells is an early event that occurs after antigen challenged,[54] the morphological changes of the cells before and after IgE-BSA complex stimulation was visualized by staining the F-actin cytoskeleton with Rhodamine-labeled phalloidin. The cells cultured on the coverslip and the GelMA hydrogel were also tested for comparison. As shown in Figure 5I, normal RBL-2H3 cells cultured on the coverslip exhibited the typical spindle shape with uniform distribution of F-actin.[55] However, after being challenged by DNP-BSA, most cells on the coverslip became larger and irregular. Especially, the cells on the GelMA hydrogel exhibited spread out morphology (Figure 5J), which was because the DNP-BSA challenging induced the disassembly of the F-actin cytoskeleton. In sharp contrast, fewer RBL-2H3 cells with membrane ruffles were observed on the PGA-GelMA hydrogels, and the cells remained in a spindle shape with a closely packed F-actin cytoskeleton even after a 1 h challenge of DNP-BSA. In addition, the exposure of RBL-2H3 cells to antigens will lead to overproduction of pro-inflammatory cytokines and lipid mediators at the late phase of allergic reaction.[55,56] Thus, the mRNA levels of interleukin-4 (IL-4) and leukotrienes C_4 (LTC_4) in RBL-2H3 cells cultured on hydrogels were further assessed by quantitative RT-PCR after the cells were challenged with DNP-BSA for 6 h (Figure 5K,L). Before DNP-BSA challenging, the mRNA levels of both IL-4 and LTC_4 in RBL-2H3 cells was almost the same in all groups, which implied that the coculturing with the PGA-GelMA hydrogel did not stimulate the allergic reactions of the RBL-2H3 cells. After the DNP-BSA challenge, the mRNA levels of IL-4 and LTC_4 in IgE-BSA complex-stimulated cells were greatly increased. Nevertheless, the PGA-GelMA hydrogel treatment significantly reduced the mRNA levels of IL-4 and LTC_4 in the RBL-2H3 cells, compared to results with the GelMA hydrogel-treated group and blank groups. These results indicated the potent antiallergic activity of PGA-GelMA hydrogels was achieved by preventing the disassembly of actin cytoskeleton and inhibiting the expression of allergy-related genes to attenuate the of IgE-mediated mast cell degranulation.

PGA-GelMA Hydrogel for Diabetic Wound Healing. The PGA-GelMA hydrogel was further applied as a therapeutic patch for wound management in a full-thickness skin defect of a type II diabetic rat model (Figure 6A). Five days after

https://doi.org/10.1021/acsnano.2c00662
ACS Nano 2022, 16, 8662−8676

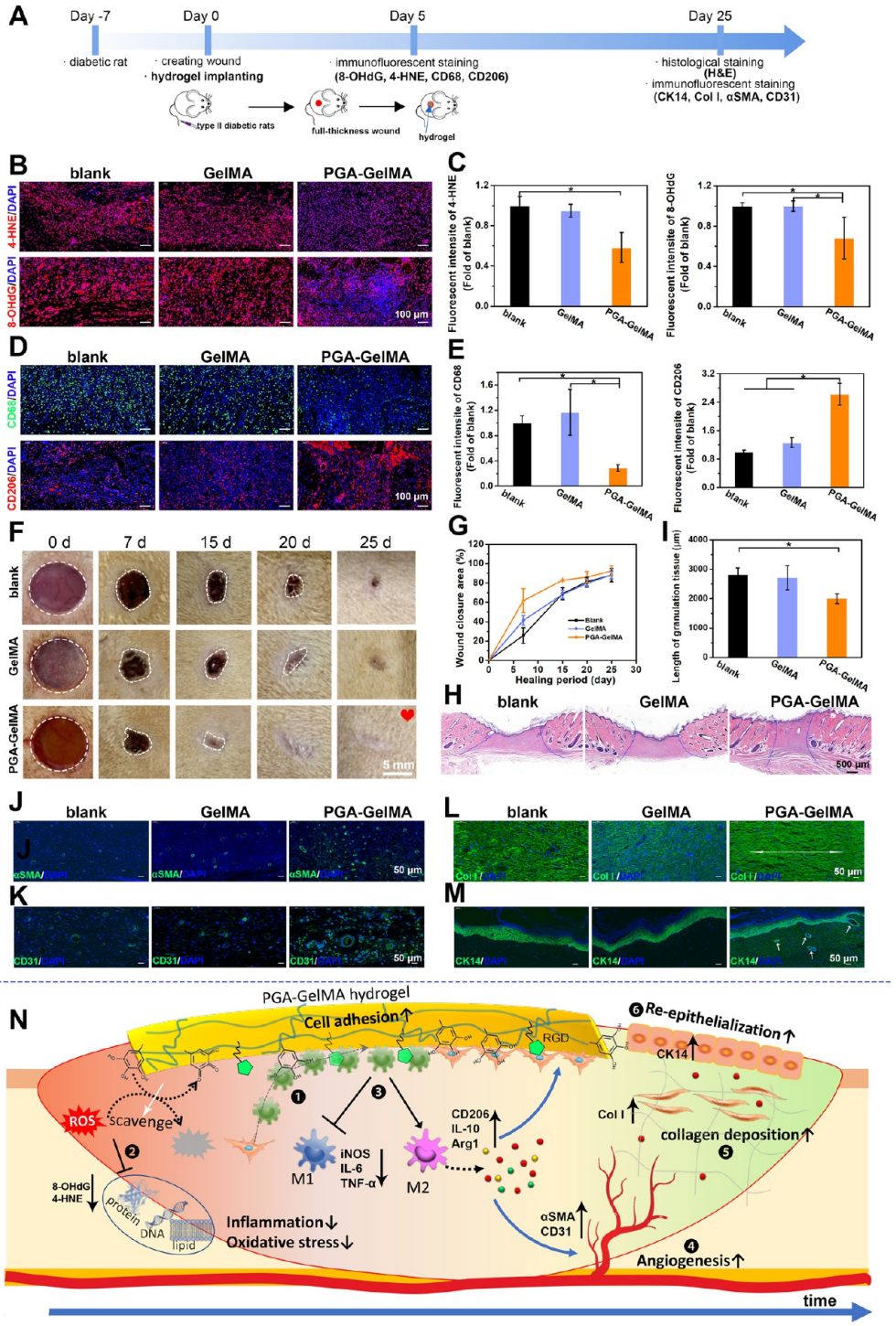

Figure 6. PGA-GelMA hydrogel accelerating wound healing and regeneration in a diabetic rat. (A) Workflow for evaluating diabetic skin wound healing, and schematic diagram of the hydrogel implanting in the wound defects. (B) Antioxidative ability of PGA-GelMA hydrogel demonstrated by immunofluorescence staining of 4-HNE (lipid peroxidation marker) and 8-OHdG (DNA damage marker) in wound samples on Day 5. (C) Quantitative analysis of the relative fluorescent intensity of 4-HNE and 8-OHdG in different groups. Data are shown as mean ± SD. (D) Anti-inflammatory and immunomodulating ability of PGA-GelMA hydrogel demonstrated by immunofluorescence staining of CD68 (green) and CD206 (red) in wound samples on Day 5. (E) Quantitative analysis of the relative fluorescent intensity of CD68 and CD206 in different groups. Data are shown as mean ± SD. (F) Digital images of the wound healing process in all groups. (G) Quantification of the wound closure area at different time intervals. (H) Representative H&E staining images of wound samples in different groups on Day 25. (I) Quantification of the length of granulation tissue. *$p < 0.05$. Immunofluorescence staining images of (J) α-smooth muscle actin (αSMA), (K) CD31, (L) collagen type I (Col I), and (M) cytokeratin 14 (CK14)-positive cells in wounds treated with different groups on Day 25. Cell nuclei were stained with DAPI (blue). White arrows in (M) showed hair follicles. (N) Schematic illustration of the PGA-GelMA hydrogel's functions during the diabetic wound healing process, including (1) promoting cell adhesion, (2) ROS scavenging, (3) anti-inflammation and immunomodulating, and facilitating (4) angiogenesis, (5) collagen deposition, and (6) re-epithelialization.

https://doi.org/10.1021/acsnano.2c00662
ACS Nano 2022, 16, 8662−8676

implantation, the hydrogel-treated wound tissues were retrieved for immunofluorescence staining using 8-hydroxydeoxyguanosine (8-OHdG) and 4-hydroxy-2-nonenal (4-HNE) to investigate the protective effect of the hydrogel on cellular components such as lipids and DNA against oxidative stress damage.[57,58] Dramatically lower 8-OHdG and 4-HNE levels were observed in the PGA-GelMA hydrogel-treated wounds than those in the blank and GelMA-treated groups (Figure 6B,C), indicating that the PGA-GelMA hydrogel could relieve oxidative stress at the initial stage of the diabetic wound healing process. Furthermore, the anti-inflammatory ability of the hydrogel was investigated by examining the infiltration and polarization of macrophages in the subcutaneous layer of the wound sites. As shown in Figure 6D, immunofluorescent staining of the CD68 marker showed a large number of macrophages (green fluorescence) in the blank group, suggesting an inflammatory status. Immunofluorescent staining also indicated that the PGA-GelMA hydrogel-treated group showed a higher expression level of CD206-positive M2 macrophages (red fluorescence), in contrast to the blank and GelMA hydrogel-treated groups (Figure 6D). Quantitative data showed that the percentage of CD206-positive M2 macrophages in wounds treated with the PGA-GelMA hydrogel was higher than that in the blank and GelMA hydrogel-treated groups (Figure 6E), confirming that the PGA-GelMA hydrogel not only suppressed the inflammation state of the wounds but also activated the macrophage polarization, therefore stimulating the wound environment in a more advanced stage of the healing process.

After a 25-day healing period, the rats were euthanized to harvest the repaired skin histological examination and immunofluorescence analysis. Digital photographs showed that the blank diabetic wounds without any treatment were difficult to fully heal even after 25 days (Figure 6F). In contrast, wounds treated with the PGA-GelMA hydrogel almost healed. The wound closure at each point was quantified, which showed that the PGA-GelMA hydrogel-treated groups exhibited the fastest wound closure rate among all the groups (Figure 6G). The healed wounds were further assessed via histological analysis of the granulation tissue gap (Figure 6H). The H&E staining indicated that the length of granulation tissue gap in the PGA-GelMA hydrogel-treated wounds was 1999 ± 164 μm, which was much smaller than that in untreated wounds (2814 ± 235 μm) and the GelMA hydrogel-treated wounds (2712 ± 408 μm) (Figure 6I).

Further immunofluorescence staining was conducted to investigate the quality and maturation of regenerated skin induced by the PGA-GelMA hydrogel. Angiogenesis was evaluated by the evident vascular endothelial-specific markers (CD31 and α-SMA) (Figure 6J,K). The results showed that the PGA-GelMA hydrogel enhanced the regeneration of new blood vessels in the wounded area, which could transport nutrition to the wound sites, being essential for wound repair. Collagen deposition in the newly regenerated skin tissue was characterized by Collagen I staining (Figure 6L). More well-organized collagen fibers were observed in the PGA-GelMA hydrogel-treated groups, which indicated that the hydrogel enhanced the secretion of type I collagen to reconstruct the structure and function of injured skin. The re-epithelialization of the regenerated skin tissue was confirmed by immunofluorescence staining of cytokeratin 14 (CK14), a type I keratin, which was mainly presented in the basal keratinocytes of the epidermis, the stratified epithelia, and the external root sheath of the hair follicles.[59,60] CK14 staining showed that the hydrogel promoted keratinized layer formation with the presence of hair follicles in the PGA-GelMA hydrogel-treated group (Figure 6M). indicating that the hydrogel had a positive effect on generating skin appendages in the healed skin tissue.

Diabetic wounds take longer to heal and increase the risk of complications because of excessive oxidative stress, prolonged inflammation response, and a dysfunctional immune system.[61−63] The PGA-GelMA hydrogel exhibited high efficiency in diabetic wound healing, which was attributed to the synergistic effect of PGA and GelMA inside the hydrogel group (Figure 6N). First, the hydrogel tightly adhered to the skin and sealed the wound, which served as an affinitive bed that recruited cells from host tissues to the injured sites. Second, the abundant polyphenol groups in the hydrogel effectively relieved the oxidative stress and reduced unresolved inflammation response, therefore reshaping the highly oxidative and inflammatory wound microenvironment.[64] Third, the hydrogel effectively modulated the polarization of macrophages to pro-healing phenotype, which further secreted growth factors and contributed to angiogenesis, collagen deposition, ECM remodeling, and re-epithelialization.[65] Moreover, GelMA in the hydrogel comprised RGD peptide sequences that are recognized by intracellular integrin receptors, which were essential for cell proliferation and crucial for skin regeneration.[66,67] With all the biofunctionalities, the hydrogel created an adhesive and favorable wound healing microenvironment, resulting in faster and better repair in diabetic wounds.

CONCLUSION

This study proposed a PGA-GelMA hydrogel as a skin-friendly bioadhesive patch that was antiallergenic and anti-inflammatory, with tunable mechanical and biodegradable properties, which was superior to conventional adhesive materials that caused damage and pain because of their aggressive adhesiveness. The hydrogel showed a balance between nondestructive adhesion and painless detachment from the skin by responding to temperature change, which was achieved via a polyphenol-GelMA complexation strategy that strengthened the thermoreversibility of the GelMA hydrogel. In addition, the hydrogel showed antioxidative and anti-inflammatory properties to prevent adhesion-caused irritation on the skin, therefore enabling nondestructive mounting and detachment of epidermal bioelectronics on infant skin for nonallergic health care. Furthermore, the hydrogel could conformally adhere to the wound sites and modulated the immune microenvironment to accelerate diabetic wound healing without encapsulation of additional drugs. In summary, this bioadhesive hydrogel with painless detachment and multiple biofunctions can potentially address the limitation of existing skin adhesives with aggressive adhesion or skin allergy symptoms, which may broaden the applications of skin adhesives to meet the increasing demands of specific end-users, such as infants, the elderly, and diabetic patients with sensitive, fragile, or vulnerable even wounded skins.

METHODS

The PGA-GelMA hydrogel was prepared via the following steps. Typically, GA (0.1 g) was first dissolved in deionized water (10 mL) to form the GA aqueous solution at 35 °C. Then NaOH (0.5 g/mL) was added to adjust the pH value of the GA solution, which allowed the oxidative polymerization of GA into PGA after 20 min of reaction. Second, GelMA (1.5 g) was dissolved in deionized DI water (8 mL) at

https://doi.org/10.1021/acsnano.2c00662
ACS Nano 2022, 16, 8662−8676

60 °C. Third, PGA solution (2 mL), PEGDA (100 μL), APS (0.2 g), and TMEDA (20 μL) were added into the GelMA solution to form the hydrogel precursor solution. After stirring for 5 min, the hydrogel precursor solution was transferred into a mold and finally polymerized to form the PGA-GelMA hydrogel. For comparison, hydrogels with different GA contents were also prepared. The specific components of the hydrogels are shown in Table S1. The detail characterizations of the PGA-GelMA hydrogels were provided in the Supporting Information.

ASSOCIATED CONTENT

Supporting Information

The Supporting Information is available free of charge at https://pubs.acs.org/doi/10.1021/acsnano.2c00662.

Experimental methods and additional figures: ESI/MS spectra, UV−vis spectra, computational calculations, temperature sweep curves, long-term adhesion on infant rat skin, conductivity and adhesive strength of hydrogel, adhesive strength of hydrogels with various GA contents and GA oxidation time, adhesive force−displacement curves, adhesion durability, compressive tests, swelling kinetics, SEM images of L929 cells on hydrogels, DPPH scavenging ability, comparisons between PGA-GelMA hydrogel and other adhesives (PDF)

PEDOT NPs-incorporated 1.3 wt % PGA-GelMA hydrogel served as bioadhesive interface for ECG recording (MP4)

Detachment of the 1.3 wt % PGA-GelMA hydrogel from scarred skin (MP4)

1.3 wt % PGA-GelMA hydrogel strongly adhered to the wounded skin even after sharply distorting (compressing, stretching, twisting) the adjacent skin (MP4)

AUTHOR INFORMATION

Corresponding Authors

Lu Han − *School of Medicine and Pharmaceutics, Laboratory for Marine Drugs and Bioproducts, Pilot National Laboratory for Marine Science and Technology, Ocean University of China, Qingdao 266003 Shandong, China*; Email: hanlu@ouc.edu.cn

Xiong Lu − *School of Materials Science and Engineering, Key Lab of Advanced Technologies of Materials, Ministry of Education, Yibin Institute of Southwest Jiaotong University, Southwest Jiaotong University, Chengdu 610031 Sichuan, China*; orcid.org/0000-0001-6367-430X; Email: luxiong_2004@163.com

Authors

Yanan Jiang − *School of Materials Science and Engineering, Key Lab of Advanced Technologies of Materials, Ministry of Education, Yibin Institute of Southwest Jiaotong University, Southwest Jiaotong University, Chengdu 610031 Sichuan, China*

Xin Zhang − *School of Materials Science and Engineering, Key Lab of Advanced Technologies of Materials, Ministry of Education, Yibin Institute of Southwest Jiaotong University, Southwest Jiaotong University, Chengdu 610031 Sichuan, China*

Wei Zhang − *School of Materials Science and Engineering, Key Lab of Advanced Technologies of Materials, Ministry of Education, Yibin Institute of Southwest Jiaotong University, Southwest Jiaotong University, Chengdu 610031 Sichuan, China*

Menghao Wang − *Department of Chemistry, Southern University of Science and Technology, Shenzhen 518055 Guangdong, China*

Liwei Yan − *School of Materials Science and Engineering, Key Lab of Advanced Technologies of Materials, Ministry of Education, Yibin Institute of Southwest Jiaotong University, Southwest Jiaotong University, Chengdu 610031 Sichuan, China*

Kefeng Wang − *National Engineering Research Center for Biomaterials, Sichuan University, Chengdu 610064 Sichuan, China*; orcid.org/0000-0002-2504-4662

Complete contact information is available at: https://pubs.acs.org/10.1021/acsnano.2c00662

Author Contributions

#Y. N. Jiang, X. Zhang, and W. Zhang contributed equally to this work.

Notes

The authors declare no competing financial interest.

ACKNOWLEDGMENTS

This work was supported by the Sichuan Key Research and Development Program of China (22ZDYF2034), NSFC (82072071, 31800798), Guangdong Basic and Applied Basic Research Foundation (2021B1515120019), Shenzhen Funds of the Central Government to Guide Local Scientific and Technological Development (2021SZVUP123), Fundamental Research Funds for Central Universities (202241010, 2682020ZT79), and the Scientific and Technological Innovation Project financially supported by the Pilot National Laboratory for Marine Science and Technology (Qingdao).

REFERENCES

(1) Hwang, I.; Kim, H. N.; Seong, M.; Lee, S. H.; Kang, M.; Yi, H.; Bae, W. G.; Kwak, M. K.; Jeong, H. E. Multifunctional smart skin adhesive patches for advanced health care. *Adv. Healthc. Mater.* **2018**, *7*, 1800275.

(2) Ma, Z.; Bao, G.; Li, J. Multifaceted design and emerging applications of tissue adhesives. *Adv. Mater.* **2021**, *33*, 2007663.

(3) Yuk, H.; Varela, C. E.; Nabzdyk, C. S.; Mao, X.; Padera, R. F.; Roche, E. T.; Zhao, X. Dry double-sided tape for adhesion of wet tissues and devices. *Nature* **2019**, *575*, 169−174.

(4) Li, J.; Celiz, A.; Yang, J.; Yang, Q.; Wamala, I.; Whyte, W.; Seo, B.; Vasilyev, N.; Vlassak, J.; Suo, Z. Tough adhesives for diverse wet surfaces. *Science* **2017**, *357*, 378−381.

(5) Zhang, Y.; Tao, T. H. Skin-friendly electronics for acquiring human physiological signatures. *Adv. Mater.* **2019**, *31*, 1905767.

(6) Zulkowski, K. Understanding moisture-associated skin damage, medical adhesive-related skin injuries, and skin tears. *Adv. Skin Wound Care* **2017**, *30*, 372−381.

(7) Pei, X.; Wang, J.; Cong, Y.; Fu, J. Recent progress in polymer hydrogel bioadhesives. *J. Polym. Sci.* **2021**, *59*, 1312−1337.

(8) Chen, X.; Yuk, H.; Wu, J.; Nabzdyk, C. S.; Zhao, X. Instant tough bioadhesive with triggerable benign detachment. *P. Natl. Acad. Sci. USA* **2020**, *117*, 15497−15503.

(9) Xie, T.; Ding, J.; Han, X.; Jia, H.; Yang, Y.; Liang, S.; Wang, W.; Liu, W.; Wang, W. Wound dressing change facilitated by spraying zinc ions. *Mater. Horizons* **2020**, *7*, 605−614.

(10) Freedman, B. R.; Uzun, O.; Luna, N. M. M.; Rock, A.; Clifford, C.; Stoler, E.; Östlund-Sholars, G.; Johnson, C.; Mooney, D. J. Degradable and removable tough adhesive hydrogels. *Adv. Mater.* **2021**, *33*, 2008553.

(11) Jiang, M.; Liu, X.; Chen, Z.; Li, J.; Liu, S.; Li, S. Near-infrared-detached adhesion enabled by upconverting nanoparticles. *Iscience* **2020**, *23*, 100832.

(12) Gao, Y.; Wu, K.; Suo, Z. Photodetachable adhesion. *Adv. Mater.* **2019**, *31*, 1806948.
(13) Huang, J.; Liu, Y.; Yang, Y.; Zhou, Z.; Mao, J.; Wu, T.; Liu, J.; Cai, Q.; Peng, C.; Xu, Y. Electrically programmable adhesive hydrogels for climbing robots. *Sci. Robot.* **2021**, *6*, abe1858.
(14) Zhao, Y.; Wu, Y.; Wang, L.; Zhang, M.; Chen, X.; Liu, M.; Fan, J.; Liu, J.; Zhou, F.; Wang, Z. Bio-inspired reversible underwater adhesive. *Nat. Commun.* **2017**, *8*, 2218.
(15) Khatsenko, K.; Khin, Y.; Maibach, H. Allergic contact dermatitis to components of wearable adhesive health devices. *Dermatitis* **2020**, *31*, 283−286.
(16) Zhao, H.; He, Y.; Wei, Q.; Ying, Y. Medical adhesive−related skin injury prevalence at the peripherally inserted central catheter insertion site: a cross-sectional, multiple-center study. *J. Wound Ostomy. Cont.* **2018**, *45*, 22−25.
(17) Lee, B. K.; Ryu, J. H.; Baek, I. B.; Kim, Y.; Jang, W. I.; Kim, S. H.; Yoon, Y. S.; Kim, S. H.; Hong, S. G.; Byun, S. Silicone-based adhesives with highly tunable adhesion force for skin-contact applications. *Adv. Healthc. Mater.* **2017**, *6*, 1700621.
(18) Cotas, J.; Leandro, A.; Monteiro, P.; Pacheco, D.; Figueirinha, A.; Gonçalves, A. M.; da Silva, G. J.; Pereira, L. Seaweed phenolics: From extraction to applications. *Mar. Drugs* **2020**, *18*, 384.
(19) Kumar, N.; Goel, N. Phenolic acids: Natural versatile molecules with promising therapeutic applications. *Biotechnol. Rep.* **2019**, *24*, No. e00370.
(20) Rasouli, H.; Farzaei, M. H.; Khodarahmi, R. Polyphenols and their benefits: a review. *Int. J. Food Prop.* **2017**, *20*, 1700−1741.
(21) Montenegro-Landívar, M. F.; Tapia-Quirós, P.; Vecino, X.; Reig, M.; Valderrama, C.; Granados, M.; Cortina, J. L.; Saurina, J. Polyphenols and their potential role to fight viral diseases: An overview. *Sci. Total Environ.* **2021**, *801*, 149719.
(22) Ding, Y.; Yang, Z.; Bi, C. W.; Yang, M.; Zhang, J.; Xu, S. L.; Lu, X.; Huang, N.; Huang, P.; Leng, Y. Modulation of protein adsorption, vascular cell selectivity and platelet adhesion by mussel-inspired surface functionalization. *J. Mater. Chem. B* **2014**, *2*, 3819−3829.
(23) Cho, J. H.; Lee, J. S.; Shin, J.; Jeon, E. J.; An, S.; Choi, Y. S.; Cho, S. W. Ascidian-inspired fast-forming hydrogel system for versatile biomedical applications: pyrogallol chemistry for dual modes of crosslinking mechanism. *Adv. Funct. Mater.* **2018**, *28*, 1705244.
(24) Giannakopoulos, E.; Isari, E.; Bourikas, K.; Karapanagioti, H.; Psarras, G.; Oron, G.; Kalavrouziotis, I. Oxidation of municipal wastewater by free radicals mechanism. A UV/Vis spectroscopy study. *J. Environ. Manage.* **2017**, *195*, 186−194.
(25) Madhan, B.; Thanikaivelan, P.; Subramanian, V.; Rao, J. R.; Nair, B. U.; Ramasami, T. Molecular mechanics and dynamics studies on the interaction of gallic acid with collagen-like peptides. *Chem. Phys. Lett.* **2001**, *346*, 334−340.
(26) Lee, Y.; Jun, K.; Lee, K.; Seo, Y. C.; Jeong, C.; Kim, M.; Oh, I. K.; Lee, H. Phenol-derived carbon sealant inspired by a coalification process. *Angew. Chem., Int. Ed.* **2020**, *59*, 3864−3870.
(27) Lin, J.; Pan, D.; Sun, Y.; Ou, C.; Wang, Y.; Cao, J. The modification of gelatin films: Based on various cross-linking mechanism of glutaraldehyde at acidic and alkaline conditions. *Food Sci. Nutr.* **2019**, *7*, 4140−4146.
(28) Young, A. T.; White, O. C.; Daniele, M. A. Rheological properties of coordinated physical gelation and chemical crosslinking in gelatin methacryloyl (GelMA) hydrogels. *Macromol. Biosci.* **2020**, *20*, 2000183.
(29) Han, L.; Lu, X.; Liu, K.; Wang, K.; Fang, L.; Weng, L.-T.; Zhang, H.; Tang, Y.; Ren, F.; Zhao, C. Mussel-inspired adhesive and tough hydrogel based on nanoclay confined dopamine polymerization. *ACS Nano* **2017**, *11*, 2561−2574.
(30) Mo, J.; Dai, Y.; Zhang, C.; Zhou, Y.; Li, W.; Song, Y.; Wu, C.; Wang, Z. Design of ultra-stretchable, highly adhesive and self-healable hydrogels via tannic acid-enabled dynamic interactions. *Mater. Horizons* **2021**, *8*, 3409−3416.
(31) Zhang, C.; Wu, B.; Zhou, Y.; Zhou, F.; Liu, W.; Wang, Z. Mussel-inspired hydrogels: from design principles to promising applications. *Chem. Soc. Rev.* **2020**, *49*, 3605−3637.
(32) Guo, Q.; Chen, J.; Wang, J.; Zeng, H.; Yu, J. Recent progress in synthesis and application of mussel-inspired adhesives. *Nanoscale* **2020**, *12*, 1307−1324.
(33) Saiz-Poseu, J.; Mancebo-Aracil, J.; Nador, F.; Busqué, F.; Ruiz-Molina, D. The chemistry behind catechol-based adhesion. *Angew. Chem., Int. Ed.* **2019**, *58*, 696−714.
(34) Zhang, C.; Zhou, Y.; Han, H.; Zheng, H.; Xu, W.; Wang, Z. Dopamine-triggered hydrogels with high transparency, self-adhesion, and thermoresponse as skinlike sensors. *ACS Nano* **2021**, *15*, 1785−1794.
(35) Rose, S.; Prevoteau, A.; Elzière, P.; Hourdet, D.; Marcellan, A.; Leibler, L. Nanoparticle solutions as adhesives for gels and biological tissues. *Nature* **2014**, *505*, 382−385.
(36) Barrett, D. G.; Bushnell, G. G.; Messersmith, P. B. Mechanically robust, negative-swelling, mussel-inspired tissue adhesives. *Adv. Healthc. Mater.* **2013**, *2*, 745−755.
(37) Sierra, D. H. Fibrin sealant adhesive systems: a review of their chemistry, material properties and clinical applications. *J. Biomater. Appl.* **1993**, *7*, 309−352.
(38) Wallace, D.; Cruise, G.; Rhee, W.; Schroeder, J.; Prior, J.; Ju, J.; Maroney, M.; Duronio, J.; Ngo, M.; Estridge, T. A tissue sealant based on reactive multifunctional polyethylene glycol. *J. Biomed. Mater. Res., Part A* **2001**, *58*, 545−555.
(39) Bergmann, N. M.; Peppas, N. A. Molecularly imprinted polymers with specific recognition for macromolecules and proteins. *Prog. Polym. Sci.* **2008**, *33*, 271−288.
(40) Koons, G. L.; Diba, M.; Mikos, A. G. Materials design for bone-tissue engineering. *Nat. Rev. Mater.* **2020**, *5*, 584−603.
(41) Annabi, N.; Rana, D.; Sani, E. S.; Portillo-Lara, R.; Gifford, J. L.; Fares, M. M.; Mithieux, S. M.; Weiss, A. S. Engineering a sprayable and elastic hydrogel adhesive with antimicrobial properties for wound healing. *Biomaterials* **2017**, *139*, 229−243.
(42) Li, M.; Liang, Y.; Liang, Y.; Pan, G.; Guo, B. Injectable stretchable self-healing dual dynamic network hydrogel as adhesive anti-oxidant wound dressing for photothermal clearance of bacteria and promoting wound healing of MRSA infected motion wounds. *Chem. Eng. J.* **2022**, *427*, 132039.
(43) Shin, M.; Lee, H.-A.; Lee, M.; Shin, Y.; Song, J.-J.; Kang, S.-W.; Nam, D.-H.; Jeon, E. J.; Cho, M.; Do, M. Targeting protein and peptide therapeutics to the heart via tannic acid modification. *Nat. Biomed. Eng.* **2018**, *2*, 304−317.
(44) Van Buren, J. P.; Robinson, W. B. Formation of complexes between protein and tannic acid. *J. Agric. Food Chem.* **1969**, *17*, 772−777.
(45) Sanders, L.; Stone, R.; Webb, K.; Mefford, T.; Nagatomi, J. Mechanical characterization of a bifunctional tetronic hydrogel adhesive for soft tissues: society for biomaterials student award winner in the graduate degree category. *J. Biomed. Mater. Res., Part A* **2015**, *103*, 861−868.
(46) Xue, B.; Gu, J.; Li, L.; Yu, W.; Yin, S.; Qin, M.; Jiang, Q.; Wang, W.; Cao, Y. Hydrogel tapes for fault-tolerant strong wet adhesion. *Nat. Commun.* **2021**, *12*, 7156.
(47) Han, L.; Yan, L.; Wang, M.; Wang, K.; Fang, L.; Zhou, J.; Fang, J.; Ren, F.; Lu, X. Transparent, adhesive, and conductive hydrogel for soft bioelectronics based on light-transmitting polydopamine-doped polypyrrole nanofibrils. *Chem. Mater.* **2018**, *30*, 5561−5572.
(48) Farokhi, M.; Mottaghitalab, F.; Fatahi, Y.; Khademhosseini, A.; Kaplan, D. L. Overview of silk fibroin use in wound dressings. *Trends Biotechnol* **2018**, *36*, 907−922.
(49) Zhou, J.; Lin, Z.; Ju, Y.; Rahim, M. A.; Richardson, J. J.; Caruso, F. Polyphenol-mediated assembly for particle engineering. *Acc. Chem. Res.* **2020**, *53*, 1269−1278.
(50) Wang, Z.; Wang, K.; Zhang, Y.; Jiang, Y.; Lu, X.; Fang, L.; Gan, D.; Lv, C.; Zhang, H.; Qu, S. Protein-affinitive polydopamine nanoparticles as an efficient surface modification strategy for versatile porous scaffolds enhancing tissue regeneration. *Part Part Syst. Char* **2016**, *33*, 89−100.
(51) Rezaei, H.; Shahrezaee, M.; Jalali Monfared, M.; Ghorbani, F.; Zamanian, A.; Sahebalzamani, M. Mussel-inspired polydopamine

https://doi.org/10.1021/acsnano.2c00662
ACS Nano 2022, 16, 8662−8676

induced the osteoinductivity to ice-templating PLGA−gelatin matrix for bone tissue engineering application. *Biotechnol. Appl. Bioc.* **2021**, *68*, 185−196.
(52) Tang, P.; Han, L.; Li, P.; Jia, Z.; Wang, K.; Zhang, H.; Tan, H.; Guo, T.; Lu, X. Mussel-inspired electroactive and antioxidative scaffolds with incorporation of polydopamine-reduced graphene oxide for enhancing skin wound healing. *ACS Appl. Mater. Interfaces* **2019**, *11*, 7703−7714.
(53) Jia, Z.; Gong, J.; Zeng, Y.; Ran, J.; Liu, J.; Wang, K.; Xie, C.; Lu, X.; Wang, J. Bioinspired conductive silk microfiber integrated bioelectronic for diagnosis and wound healing in diabetes. *Adv. Funct. Mater.* **2021**, *31*, 2010461.
(54) Dráber, P.; Sulimenko, V.; Dráberová, E. Cytoskeleton in mast cell signaling. *Front. Immunol.* **2012**, *3*, 130.
(55) Tan, J. W.; Israf, D. A.; Harith, H. H.; Hashim, N. F. M.; Ng, C. H.; Shaari, K.; Tham, C. L. Anti-allergic activity of 2, 4, 6-trihydroxy-3-geranylacetophenone (tHGA) via attenuation of IgE-mediated mast cell activation and inhibition of passive systemic anaphylaxis. *Toxicol. Appl. Pharmacol.* **2017**, *319*, 47−58.
(56) Wang, W.; Zhou, Q.; Liu, L.; Zou, K. Anti-allergic activity of emodin on IgE-mediated activation in RBL-2H3 cells. *Pharmacol. Rep.* **2012**, *64*, 1216−1222.
(57) Marrocco, I.; Altieri, F.; Peluso, I. Measurement and clinical significance of biomarkers of oxidative stress in humans. *Oxid. Med. Cell Longev.* **2017**, *2017*, 6501046.
(58) Dhama, K.; Latheef, S. K.; Dadar, M.; Samad, H. A.; Munjal, A.; Khandia, R.; Karthik, K.; Tiwari, R.; Yatoo, M.; Bhatt, P. Biomarkers in stress related diseases/disorders: diagnostic, prognostic, and therapeutic values. *Front. Mol. Biosci.* **2019**, *6*, 91.
(59) Kumar, A.; Jagannathan, N. Cytokeratin: A review on current concepts. *Inter. J. Orofacial Biology* **2018**, *2*, 6.
(60) Meizarini, A.; Aryati, A.; Rianti, D.; Riawan, W.; Puteri, A. Effectivity of zinc oxide-turmeric extract dressing in stimulating the reepithelization phase of wound healing. *Vet. World* **2020**, *13*, 2221.
(61) Matoori, S.; Veves, A.; Mooney, D. J. Advanced bandages for diabetic wound healing. *Sci. Transl. Med.* **2021**, *13*, abe4839.
(62) Liang, Y.; He, J.; Guo, B. Functional hydrogels as wound dressing to enhance wound healing. *ACS Nano* **2021**, *15*, 12687−12722.
(63) Guo, B.; Dong, R.; Liang, Y.; Li, M. Haemostatic materials for wound healing applications. *Nat. Rev. Chem.* **2021**, *5*, 773−791.
(64) Han, L.; Li, P.; Tang, P.; Wang, X.; Zhou, T.; Wang, K.; Ren, F.; Guo, T.; Lu, X. Mussel-inspired cryogels for promoting wound regeneration through photobiostimulation, modulating inflammatory responses and suppressing bacterial invasion. *Nanoscale* **2019**, *11*, 15846−15861.
(65) Liu, S.; Zhang, Q.; Yu, J.; Shao, N.; Lu, H.; Guo, J.; Qiu, X.; Zhou, D.; Huang, Y. Absorbable thioether grafted hyaluronic acid nanofibrous hydrogel for synergistic modulation of inflammation microenvironment to accelerate chronic diabetic wound healing. *Adv. Healthc. Mater.* **2020**, *9*, 2000198.
(66) Hosoyama, K.; Lazurko, C.; Muñoz, M.; McTiernan, C. D.; Alarcon, E. I. Peptide-based functional biomaterials for soft-tissue repair. *Front. Bioeng. Biotechnol.* **2019**, *7*, 205.
(67) Dhavalikar, P.; Robinson, A.; Lan, Z.; Jenkins, D.; Chwatko, M.; Salhadar, K.; Jose, A.; Kar, R.; Shoga, E.; Kannapiran, A. Review of integrin-targeting biomaterials in tissue engineering. *Adv. Healthc. Mater.* **2020**, *9*, 2000795.

https://doi.org/10.1021/acsnano.2c00662
ACS Nano 2022, 16, 8662−8676